SMR.858 - 26

I

SUMMER SCHOOL IN HIGH ENERGY PHYSICS AND COSMOLOGY

12 June - 28 July 1995

QCD AND RELATED TOPICS

I. HINCHLIFFE
Lawrence Berkeley Lab.
University of California
Berkeley, CA 94720
USA

Applications of QCD to Hadron-Hadron Collisions: Theoretical. *

Ian Hinchliffe

Lawrence Berkeley Laboratory
University of California
Berkeley, California 94720

Abstract

I discuss some current problems associated with the applications of QCD to
event rates in high energy collisions. Emphasis is given to the current ambiguities
and uncertainties that exist in estimates of signals and backgrounds.

1 Introduction

In these lectures, I shall provide an introduction to perturbative QCD and its
uses in calculating rates at hadron-hadron colliders. Since QCD processes account
for most of the background for new physics at such colliders, it is important to
understand the uncertainties in these predicted rates. Given the limited time
available I have had to be selective in the topics discussed.[1] I will begin with a
discussion of the one parameter of QCD, namely, its coupling constant. I shall
then discuss the parton model in some detail. After a discussion of the appropriate
kinematical variables I shall discuss the uncertainties and ambiguities inherent
in QCD calculations. I shall then discuss some aspects of jet physics and will end
with a discussion of underlying (minimum bias) events.

2 QCD and the parton model

The QCD Lagrangian may be written as follows:

$$-\frac{1}{4}F^i_{\mu\nu}F^i_{\mu\nu} + \sum_j \bar{\psi}_j(i\,\not{D} - m_j)\psi_j. \tag{1}$$

The sum on j runs over quark flavors and,

$$F^i_{\mu\nu} = \partial_\mu G^i_\nu - \partial_\nu G^i_\mu - ig f_{ijk}G^j_\mu G^k_\mu \tag{2}$$

---

[1]For a more detailed discussion see ref. [1]

and

$$D_\mu = \partial_\mu - ig\, t^i\, G_\mu^i. \tag{3}$$

Here t^i are the 3×3 representation matrices and the structure constants f_{ijk} are given by $[t_i, t_j] = if_{ijk}t_k$.

Apart from the quark masses, which have their origin in the Weinberg-Salam model of weak interactions, the theory has only one fundamental parameter, the coupling constant g. It is this coupling constant that provides us with an expansion parameter. If calculations are undertaken beyond the leading order in the coupling constant, ultra-violet divergences are encountered. These divergences must be regulated and reabsorbed into the fundamental parameters of the theory, i.e. the theory must be renormalized and a renormalized coupling constant defined. The easiest scheme for regulating and defining a coupling constant is the modified minimal subtraction scheme ($\overline{MS}$) [2]. The ultra violet divergences are regulated by calculating with the theory in n dimensions [3].

In order to understand the procedure, let us calculate a physical process $P(Q^2)$, which depends on some energy scale Q; P could, for example, represent a cross-section. It is convenient to choose the quantity P to be dimensionless; this can always be done by multiplying it by an appropriate power of Q. If we neglect quark masses, calculate in n dimensions then

$$P(Q^2) \sim \left[\frac{2A}{4-n} - A\gamma_E + A\log 4\pi - F(\mu, Q^2, g) \right]. \tag{4}$$

Here A is some constant and F a function that is finite when $n = 4$. The scale μ is introduced so that the coupling constant g remains dimensionless in n dimensions, viz.,

$$g \to g\mu^{(4-n)/2}. \tag{5}$$

The ultra-violet divergences appear as singularities at $n = 4$. The $\overline{MS}$ scheme is defined by removing the terms of the form $1/(n-4)$, γ_E and $\log 4\pi$. Then P has the form

$$P(Q^2) = F(Q^2/\mu^2, \alpha). \tag{6}$$

I have replaced g by α: $\alpha \equiv g^2/4\pi$ and the coupling constant is now in the $\overline{MS}$ scheme. The scale μ is arbitrary so that a physical quantity cannot depend upon its value

$$\frac{dP}{d\mu} = 0 \tag{7}$$

which implies

$$\left(\mu^2 \frac{\partial F}{\partial \mu^2} + \beta(\alpha)\frac{\partial F}{\partial \alpha} \right) = 0. \tag{8}$$

Here $\beta(\alpha)$ is defined by

$$\beta(\alpha) \equiv \mu^2 \frac{\partial \alpha}{\partial \mu^2}. \tag{9}$$

We can introduce a momentum-dependent coupling $\alpha(t)$ via

$$t \equiv \int_\alpha^{\alpha(t)} \frac{dp}{\beta(p)} \tag{10}$$

where $t = \log(Q^2/\mu^2)$. Then Equation 8 has the solution

$$F(t, \alpha) = F(1, \alpha(t)). \tag{11}$$

Hence the only dependence on the scale Q or t is carried by $\alpha(t)$. We can expand β as a power series in α.

$$\beta = -b\frac{\alpha}{4\pi} - b'(\frac{\alpha}{4\pi})^2 + \dots \tag{12}$$

Hence $\alpha(\mu^2)$ has the following form:

$$\alpha(\mu^2) = \frac{4\pi}{b\log(\mu^2/\Lambda^2)} + \dots \tag{13}$$

Here $b = 11 - 2n_f/3$ where n_f is the number of quark flavors with mass less than μ. We can regard the fundamental parameter of QCD either as $\alpha(Q_0^2)$ or as the scale Λ. Notice that as μ becomes small, α becomes large. Therefore, perturbation theory cannot be used to discuss processes which involve momentum flows as small as a few times Λ.

Other renormalization schemes are possible, for example one could not subtract the γ_E and $\log 4\pi$ terms. A physical quantity is, of course, independent of the renormalization scheme. However, if the perturbation series is terminated at some finite order in the coupling constant, the values of P (P_N) calculated to this order in two difference schemes will differ

$$P_N(\bar{\alpha}) \neq P_N(\alpha) = P_N(\bar{\alpha}) + 0(\alpha^{N+1}). \tag{14}$$

Since the coupling constant of QCD is not very small and most processes are not known to a very high order, these differences can be significant.

As a specific example of QCD process, consider the total cross-section for $e^+e^- \to$ hadrons at center-of-mass energy $\sqrt{s}$. In the one photon approximation (see Figure 1) this is given by

$$\sigma_{had} = \frac{8\pi\alpha_{em}^2}{3s^2} \sum_n (2\pi)^4\delta(q - q_n)\langle 0|j_\mu|n\rangle\langle n|j_\mu|0\rangle \tag{15}$$

where j_μ is the electromagnetic current of the quarks

$$j_\mu = \sum_i e_i \bar{\psi}_i \gamma_\mu \psi_i. \tag{16}$$

If we introduce the photon self-energy function $\Pi^{\mu\nu}$

$$\Pi_{\mu\nu}(q) = i \int d^4x e^{iqx} \langle 0 | T(j_\mu(x) j_\nu(0)) | 0 \rangle. \tag{17}$$

Defining $\Pi_{\mu,\nu}(q) = (g_{\mu,\nu}q^2 - q_\mu q_\nu) = \Pi(Q^2)$ then

$$\sigma_{had} = \frac{16\pi^2 \alpha_{em}^2}{s} \, Im \, \Pi(s). \tag{18}$$

A dimensionless quantity is $R(s)$ defined by

$$R(s) = \frac{\sigma_{had}}{\sigma(e^- e^+ \to \mu^+ \mu^-)} . \tag{19}$$

The previous argument implies that $R = R(\alpha(s))$. If we calculate R using perturbation theory we get

$$R = \sum e_i^2 \left(1 + \frac{\alpha_s}{\pi} + B \left(\frac{\alpha_s}{\pi} \right)^2 \dots \right) \tag{20}$$

where the sum runs over all quarks (electric charge e_i) of mass less than $\sqrt{s}/2$ and B is a scheme-dependent constant which is small in the $\overline{MS}$ scheme [4].

In order to discuss processes which involve hadrons in the initial state, we must discuss the parton model. Consider the case of electron-proton scattering, where the cross-section can be written as

$$\frac{d\sigma}{dxdy} = \frac{4\pi \alpha_{em}^2 s}{Q^4} \left[\frac{1 + (1-y)^2}{2} 2x F_1(x, Q^2) + (1-y)(F_2(x, Q^2) - 2x F_1(x, Q^2)) \right] \tag{21}$$

The variables are defined as follows (see Figure 2): q is the momentum of the exchanged photon and P is the momentum of the target proton and k is that of the incoming electron

$$
\begin{aligned}
Q^2 &= -q^2 \\
\nu &= \frac{q \cdot P}{m_p} \\
x &= \frac{Q^2}{2 m_p \nu} \\
y &= \frac{q \cdot p}{k \cdot p} \\
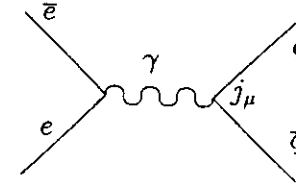s &= 2p \cdot k + m_p^2
\end{aligned}
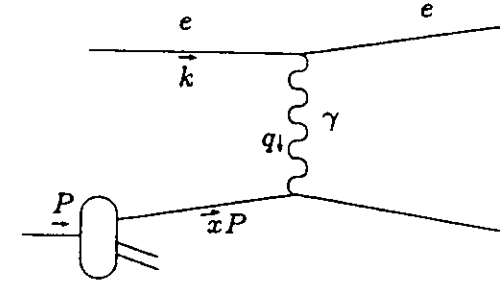\tag{22}
$$

Figure 1: Feynman graph for $e^+ e^- \to$ hadrons.

Figure 2: Diagram illustrating the variables in deep inelastic scattering (see Equation 21): electron + proton $\to$ electron + anything.

where m_p is the proton mass. I have neglected parity violating effects which arise from the exchange of a Z boson instead of a photon.

In the naive parton model the proton is viewed as being made up of a set of non-interacting partons. The structure functions F_1 and F_2 are related to the probability distribution $q_i(x)$ which represents the probability of finding a parton of type i (quark or gluon) inside the proton with fraction x of the proton's momentum, and the scattering cross-section for such a virtual photon from a parton:

$$F_1 = \frac{F_2}{2x} = \sum_i \int_x^1 \frac{dy}{y} q_i(y)[e_i^2 \delta(x/y - 1)] \tag{23}$$

where e_i is the charge of parton of type i. The δ-function appears from the cross-section for $q + \gamma \to q$ and corresponds to the constraint that the massless quark in the final state is on mass-shell. Let us consider QCD corrections to this scattering. At next order in α_s, there are contributions from gluon emission which lead to the final state $q + g$ and also from virtual gluons (see Figure 3). To order α_s Equation 23 is replaced by

$$F_1 = \sum_i \int_x^1 \frac{dy}{y} q_i(y) \left[e_i^2 \delta\left(\frac{x}{y} - 1\right) + \sigma_i\left(\frac{x}{y}, Q^2\right) \right] \tag{24}$$

with

$$\sigma_i(z, Q^2) = \frac{\alpha_s}{2\pi} e_i^2 \left[t P_{qq}(z) + f(z) + 0\left(\frac{1}{Q^2}\right) \right] \tag{25}$$

and

$$P_{qq}(z) = \frac{4}{3} \frac{(1 + z^2)}{1 - z} \tag{26}$$

for $z \neq 1$. Here $t = \log(Q^2/\mu^2)$ and the scale μ has appeared from dimensional regularization (I have dropped terms proportional to $1/(n-4)$). The μ dependence arises because σ_i is not finite in four dimensions. In the cases discussed previously, the divergences arose from large momentum flows inside loop diagrams (ultra-violet divergences). In this case these divergences cancel. Individual Feynman diagrams can also have divergences when momentum flows become very small or particles are collinear. The former (soft) divergences cancel between the real and the virtual diagrams but the collinear ones do not. It is these divergences that appear as singularities in the calculation of F_1 and are responsible for the μ dependence in Equation 25. In order to see the origin of the problem consider the graph of Figure 3 and work in a frame where $k_\mu = (k, k, 0, 0)$.

If the transverse momentum of the gluon (p) relative to k is small then we can take $p = (\eta k + k_\perp^2/2\eta k, \eta k, k_\perp 0)$. (Terms of order $k_\perp^2$ are neglected.) The internal quark line now has invariant mass squared $r^2 = (k - p)^2 = k_\perp^2/\eta$, so that
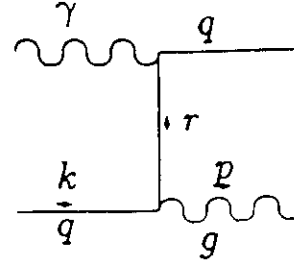

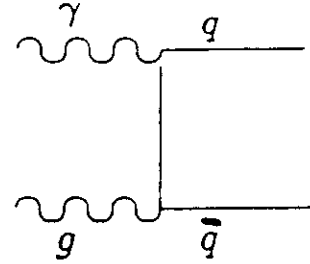Figure 3: Diagram contributing to the process $q + \gamma \to X$ at order α_s.

Figure 4: Diagram showing $g + \gamma \to q + \bar{q}$.

the squared amplitude from the graph will contain $1/k_\perp^4$. Now, at very small $k_\perp$ helicity conservation forbids the emission of a real gluon from a quark line, so that one factor of $k_\perp^2$ appears in the numerator. We now have for the total cross-section $q + \gamma \to q + $ anything, a contribution

$$\sigma \sim \frac{\alpha_s}{2\pi} \int \frac{dk_\perp^2}{k_\perp^2} \tag{27}$$

which gives rise to a logarithmic singularity. Notice that for a massive quark the singularity becomes $\log(Q^2/m_q^2)$.

We have obtained a result which depends on μ (or contains the large $\log(Q^2/m_q^2)$ if quark masses are retained). This is not physically meaningful. But Equation 24 contains the unknown quantity $q_i(y)$. We can define

$$q_i(x,t) = q_i(x) + \frac{\alpha_s t}{2\pi} \int_x^1 \frac{dy}{y} q(y) P_{qq}\left(\frac{x}{y}\right). \tag{28}$$

Hence

$$F_1 = \sum_i \int_x^1 e_i^2 \frac{dy}{y} q_i(y) \left[\delta\left(\frac{x}{y} - 1\right) + \frac{\alpha_s}{2\pi} f\left(\frac{x}{y}\right) \right] + 0(\alpha^2). \tag{29}$$

The t dependence can be eliminated at the cost of introducing a t-dependent structure function.

I have so far considered an oversimplification of the true problem. To order α_s there is an additional partonic process, namely $gluon + \gamma \to q + \bar{q}$ (see Figure 4). This process also contains a log (Q^2/μ^2) arising from the propagation of the internal quark close to its mass shell. This singularity results in the replacement of Equation 24 and 25 by

$$F_1(x,t) = \int_x^1 \frac{dy}{y} \left[\sum_i e_i^2 q_i(y) \left[\delta(\frac{x}{y}) + \frac{\alpha_s}{2\pi} \left[t P_{qq}(\frac{x}{y}) + f_q(\frac{x}{y}) \right] \right] \right.$$
$$\left. + (\sum_i e_i^2) g(y) \frac{\alpha_s}{2\pi} \left[t P_{qg}(\frac{x}{y}) + f_g(\frac{x}{y}) \right] \right]$$

with $P_{qg}(x) = 1/2(x^2 + (1-x)^2)$. The t dependence can be absorbed by defining

$$q_i(x,t) = q_i(x) + \frac{\alpha_s}{2\pi} t \int_x^1 (q_i(y) P_{qq}(\frac{x}{y}) + g(y) P_{qg}(\frac{x}{y})) \frac{dy}{y} \tag{30}$$

so that the quark and gluon distributions ($q_i(x)$ and $g(x)$) are now coupled. This equation can be recast in the more familiar form (Altarelli-Parisi equations) [5]

$$\frac{dq_i(x,t)}{dt} = \frac{\alpha_s(t)}{2\pi} \int_x^1 (q_i(y) P_{qq}(\frac{x}{y}) + g(y) P_{qg}(\frac{x}{y})) \frac{dy}{y}. \tag{31}$$

The equation for the evolution of the gluon distribution is

$$\frac{dg_i(x,t)}{dt} = \frac{\alpha_s(t)}{2\pi} \int_x^1 (q_i(y) P_{gq}(\frac{x}{y}) + g(y) P_{gg}(\frac{x}{y})) \frac{dy}{y}. \tag{32}$$

Given data from which $q_i(x,t_0)$ and $g(x,t_0)$ can be obtained as functions of x for a fixed t_0, these equations for the evolution of $q(x,t)$ and $g(x,t)$ with t can be solved to obtain them for all t. Note that structure functions at x_1 and t_1 depend only on those at $x > x_1$ provided $t_1 > t_0$. Since these equations are valid only to lowest order in α_s, t_0 must be sufficiently large for $\alpha_s(t_0)$ to be small enough so that the perturbation series can be trusted. If the equations are used to extrapolate to $t > t_0$ the series will become more trustworthy. The order α_s^2 terms in the Altarelli-Parisi equations are known and are included in some parameterizations of $q_i(x,t)$ (see below). The structure functions fall to zero as x tends to 1 (see Figure 5).

Before leaving the Altarelli-Parisi equations, I would like to discuss the behaviour of the structure functions at very small values of x. As the energy available increases it becomes possible to reach smaller and smaller values of x at fixed Q^2. Consider the behaviour of the gluon distribution at small x. We can neglect the generation of gluons from quarks since the gluon density is larger at small x (see Figure 5). The Altarelli-Parisi equation simplifies to

$$\frac{d}{dt} g(x,t) = \frac{\alpha_s}{2\pi} \int_x^1 \frac{dy}{y} g(y,t) P_{gg}\left(\frac{x}{y}\right). \tag{33}$$

Furthermore $P_{gg}(x)$ may be approximated by

$$P_{gg}(x) = \frac{6}{x}. \tag{34}$$

Equation 33 can be recast as

$$-x \frac{d^2(xg(x,t))}{dx d\log t} = \frac{12}{b} xg(x,t). \tag{35}$$

Here I have eliminated $\alpha_s(q^2)$ using Equation 13. Equation 35 can be solved to give

$$xg(x,Q^2) \propto exp\left(\sqrt{\frac{48}{b} \log(1/x) \log\log(Q^2)} \right). \tag{36}$$

The growth of this at small x is very rapid. It is eventually cut off when the equations break down [6]. We can estimate the position of this breakdown as follows. The Altarelli Parisi equations describe the growth of incoherent parton showers: the shower initiated by one parton is independent of that of the other

partons. This assumption must eventually break down. Let us view the proton in a frame which is moving extremely fast, the appropriate frame for the parton picture. The proton looks like a pancake with area $1/m_\pi^2$. Viewed on a scale Q^2 it contains a set of partons each of size $1/Q$. The fractional area occupied by partons is

$$\frac{xg(x, Q^2)m_\pi^2}{Q^2}. \tag{37}$$

Provided this fraction is small the partons are not densely packed and the incoherent approximation is correct. If the fraction is of order one, the incoherent approximation breaks down and the growth of $g(x, Q^2)$ is cut off.

A vital property of QCD is that the distribution functions defined by Equation 28 are universal. In order to illustrate this, consider the Drell-Yan process in proton-proton collisions. In the naive parton model, the cross-section for the production of a $\mu^+\mu^-$ pair of invariant mass M in a proton-proton collision (the Drell-Yan process) with total center-of-mass energy $\sqrt{s}$ is given by

$$\frac{d\sigma}{dM^2} = \frac{4\pi\alpha_{em}^2}{9M^2s} \int dx_1 dx_2 [\sum_i q_i(x_1)\bar{q}_i(x_2)e_i^2\delta(x_1x_2 - M^2/s) + (1 \Leftrightarrow 2)]. \tag{38}$$

Here $\bar{q}$ is an antiquark distribution. The fundamental process is quark-antiquark annihilation into $\mu^+\mu^-$. Consider the corrections to this at order α_s. As in the case of ep scattering these can involve either virtual or real gluons (see Figure 6). These corrections modify Equation 38, viz.,

$$\frac{d\sigma}{dM^2} = \frac{4\pi\alpha_{em}^2}{9M^2s} \int \frac{dx_1}{x_1}\frac{dx_2}{x_2} [[e_i^2 q_i(x_1)\bar{q}_i(x_2) + (1 \Leftrightarrow 2)]$$

$$\left[\delta(1-z) + \theta(1-z)\frac{\alpha_s}{2\pi}[2P_{qq}(z)t + f'(z)]\right]$$

$$+ [\sum_i e_i^2(q_i(x_1) + \bar{q}_i(x_1))G(x_2) + (1 \Leftrightarrow 2)]$$

$$[\theta(1-z)\frac{\alpha_s}{2\pi}[P_{qg}(z) + f''(z)] \tag{39}$$

where $z = M^2/(sx_1x_2)$ [7]. The last part of the expression arises from the process $g + q \rightarrow \mu^+\mu^- + q$.

If we replace $q(x)$ by $q(x, t)$ defined by Equation 28 then the resulting expression will have no t's appearing explicitly, viz.,

$$\frac{d\sigma}{dM^2} = \frac{4\pi\alpha_{em}^2}{9M^2s} \int dx_1 dx_2 [e_i^2 q_i(x_1, t)\bar{q}_i(x_2, t)\delta(x_1x_2 - M^2/s) + (1 \Leftrightarrow 2) + \mathcal{O}(\alpha_s(Q^2))] \tag{40}$$

where the order $\alpha_s(Q^2)$ terms contain no powers of t. This absorption of the singular terms into $q(x, t)$ is known as factorization; it is a universal property
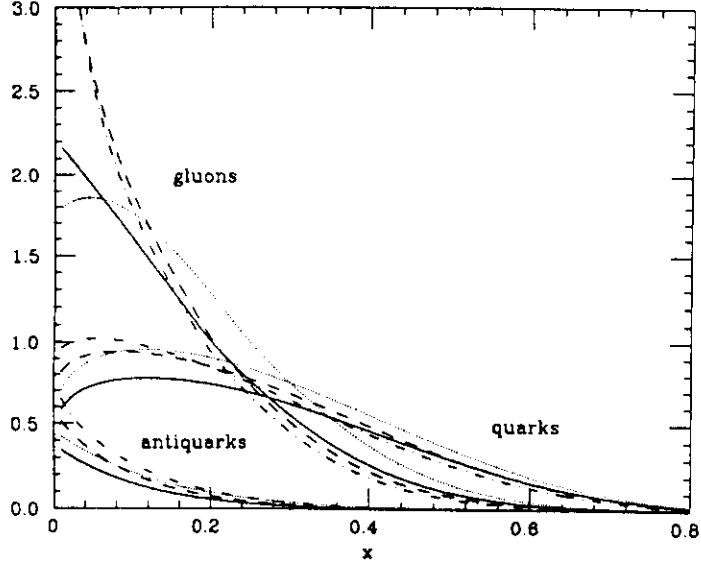

Figure 5: Diagram showing the behavior of the quark and gluon distributions as functions of x for various Q^2. Plotted is $xf(x)$ for gluons, quarks and antiquarks (summed over quark flavors). The solid (dotted) lines correspond to the structure functions of Reference [24]([20]) at $Q^2 = 5$ GeV^2. The dashed (dot-dashed) lines correspond to these structure functions evolved to $Q^2 = 25$ GeV^2 using QCD.

which guarantees that hard processes can be reliably calculated in perturbative QCD and that the same set of structure functions should be used for all processes [8].

In summary, all cross-sections involving the transfer of large momentum (greater than 10 GeV) or the production of heavy particles can be calculated using the parton model. The cross-sections are given by

$$\sigma = \sum_{i,j} \int dx_1 dx_2 f_i(x_1, Q^2) f_j(x_2, Q^2) \hat{\sigma}_{ij} \qquad (41)$$

where the sum runs over the parton types (quarks and gluons) and $\hat{\sigma}_{ij}$ is the cross-section involving partons that is calculated using perturbative QCD. Many partonic processes involve $2 \to 2$ processes of the type $a+b \to c+d$. In these cases is is useful to write the partonic cross-section in terms of Mandelstam variables: $s = (p_a + p_b)^2$, $t = (p_a - p_c)^2$, and $u = (p_b - b_c)^2$.

3 Structure of hadron-hadron events

Particle production in pp interactions is best described in terms of a particle's transverse momentum (P_t, a two dimensional vector in the plane orthogonal to the beam) and its rapidity. The latter is defined by

$$y = \frac{1}{2} log(\frac{E + P_l}{E - P_l}) \qquad (42)$$

where P_l is the component of the particle's momentum along the beam direction. Also useful is the pseudorapidity (η) defined in terms of the angle that the particle makes with the beam (θ) by

$$\eta = -log(tan(\theta/2). \qquad (43)$$

For a massless particle $\eta = y$. For a particle of mass M, the maximum rapidity is $y_{max} = log(\sqrt{s}/M)$. In terms of these variables the invariant phase space element is

$$\frac{d^3p}{E} = p_t dp_t dy d\phi \qquad (44)$$

where ϕ is the azimuthal angle and $p_t = |P_t|$. Rapidity is an additive quantity in the following sense. If a particle A is produced with rapidity y_A in the pp center-of-mass and decays so that one of its decay products (B) has rapidity y_B in the rest frame of A, then the rapidity of B in the pp center-of-mass frame is $y_A + y_B$.

The dominant part of the cross-section in pp or $p\bar{p}$ collisions at currently available energies consists of production of particles (so called minimum bias events)
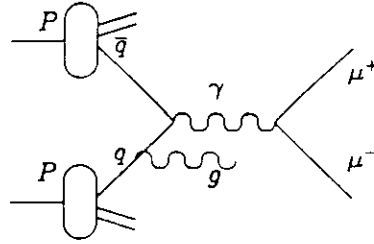

Figure 6:   Feynman graph illustrating an order α_s contribution to the Drell-Yan process (see Equation 39).

that are distributed approximately uniformly in rapidity and have a transverse momentum spectrum that falls rapidly with increasing p_t. As $\sqrt{s}$ increases from 630 GeV to 1.8 TeV, the average value of p_t rises from 432 ± 4 MeV to 495 ± 14 MeV, while $dn/d\eta$ increases by a factor of 1.27 ± 0.4 from its value of $3.30 \pm .15$ at 630 GeV[53].

The production cross-section for heavy particles at hadron colliders is also flat in rapidity near $y = 0$. The reason for this can be understood from the example of W production, the cross section for which has the following form

$$d\sigma \sim dx_1 dx_2 q(x_1, M_W^2) \bar{q}(x_2, M_W^2) \delta(x_1 x_2 - M_W^2/s). \tag{45}$$

The longitudinal momentum of the W is $(x_1 - x_2)\sqrt{s}/2$ and its transverse momentum is zero. Hence if we define $\tau = x_1 x_2$, we can write x_1 and x_2 in terms of the rapidity (y_W) of the W:

$$x_1 = \sqrt{\tau} e^{y_W}, \quad x_2 = \sqrt{\tau} e^{-y_W} \tag{46}$$

and $dx_1 dx_2 = dy_W d\tau$. The structure functions can be parameterized approximately by

$$f(x) \sim x^a (1 - x)^b. \tag{47}$$

Hence

$$\frac{d\sigma}{dy} \sim \tau^a (1 + \tau - \sqrt{\tau}\cosh y_W)^b. \tag{48}$$

Hence $d\sigma/dy_W$ is almost constant if $\sqrt{\tau}\cosh y_W \lesssim 0.1$. In the case of W production the Tevatron $\sqrt{\tau} \sim 0.04$ and hence $d\sigma/dy_W$ should be approximately flat for $|y| \lesssim 1.5$. Figure 7 shows the cross-section. It can be seen from this figure that the naive expectation is in agreement with the exact calculation.

4 Uncertainties in Predicted Rates

I will now turn to the errors and uncertainties inherent in QCD predictions at hadron-hadron colliders. In order to calculate a cross-section, one needs; structure functions; α_s; the partonic cross-section and a jet definition if the process has jets in the final state. The current value of $\Lambda_{\overline{MS}}$ quoted by the Particle Data Group[10] is 180 ± 95 MeV. The corresponding $\alpha_s(Q)$ is shown as a function of Q in Figure 8. It can be seen that the corresponding uncertainty in α_s is order 15% independent of Q. Since a cross-section for n jets in a hadron-hadron collision is proportional to α_s^n, it will be uncertain by $n \times 15\%$. The situation is slightly better in e^+e^- collisions where the uncertainty is of order $(n - 2) \times 15\%$.
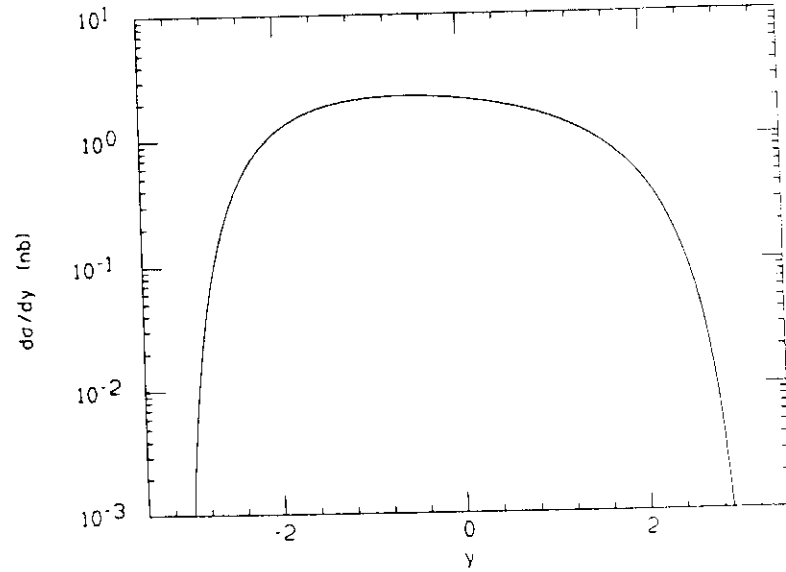

Figure 7:   Figure showing the cross-section $d\sigma/dy_W$ for the production of a W^+ as a function of the rapidity of the W^+ in $p\bar{p}$ interactions at $\sqrt{s} = 1.8 TeV$.

A detailed discussion of the determination of the distribution functions and an estimate of the errors in them can be found in Ref. [11]. The existing parameterizations arise from fits to deep inelastic scattering data (with occasional input from Drell-Yan and photon production in hadron collisions). One of the major difficulties with such fits is the systematic disagreement between different data sets. This problem is illustrated in Figure 9 which shows a comparison of $F_2(x, Q^2)$ as measured by EMC[12], BCDMS[13] and SLAC[14] data on a hydrogen target. The EMC and BCDMS experiments cover the same kinematic range but do not agree. BCDMS is higher at small x and lower at large x than EMC. The ratio of them is approximately independent of Q^2. It is not clear which of these data provides a better extrapolation of the SLAC data into the range of larger Q^2. A comparison of the EMC[15] data on an iron target with the BCDMS[16] data on carbon reveals similar systematic differences. The results of these two measurements show systematic differences that are larger than the quoted errors [17]. When using these data to extract distribution functions, a choice must be made between them.

There are many sets of distribution functions coming from fits to the data using lowest order QCD. The most frequently used of these are the two sets of Duke and Owens [18] (DO1 and DO2) which were based on data from EMC [15], SLAC [14] and CDHS [20] [25] (the latter were renormalized in an attempt to deal with the systematic differences in the data sets, see above), and Eichten *et al.* [19] (EHLQ1 and EHLQ2) based primarily on the CDHS data [20]. These pairs correspond to different shapes for the gluon distribution and consequently different values of α_s (or Λ). As usual, the gluon distribution with more support at large x (harder distribution) corresponds to the larger value of α_s (EHLQ2 and DO2). Parameterizations of these distribution functions are given in the papers and can easily be applied to a variety of other processes.

Recently, fits using next-to-leading order QCD have emerged. Diemoz, Ferroni, Longo and Martinelli (DFLM) [21] used neutrino data from BEBC [22] , CCFRR [23], CHARM [24] and CDHS [20] [25]. They also provide different fits corresponding to different values of α_s. They give sets of distribution functions corresponding to a range of $\Lambda^{\ddagger}$ viz $\Lambda = 160, 260, 360$ MeV. These fits are used to estimate the uncertainties in top quark rates at the Tevatron and $Sp\bar{p}S$ colliders [26].

Martin, Roberts and Stirling (MRS) [27] have used EMC data together with

---

‡Here we are quoting a Λ that corresponds to 4 flavors, in the range $m_{charm} < Q < m_{bottom}$ the formula for α_s is $\alpha_s(Q^2) = \frac{12\pi}{25\log(Q^2/\Lambda^2)}[1 - \frac{462}{625}\frac{\log\log(Q^2/\Lambda^2)}{\log(Q^2/\Lambda^2)}]$. See reference [10] for a summary of the behavior of this formula as a threshold is crossed.
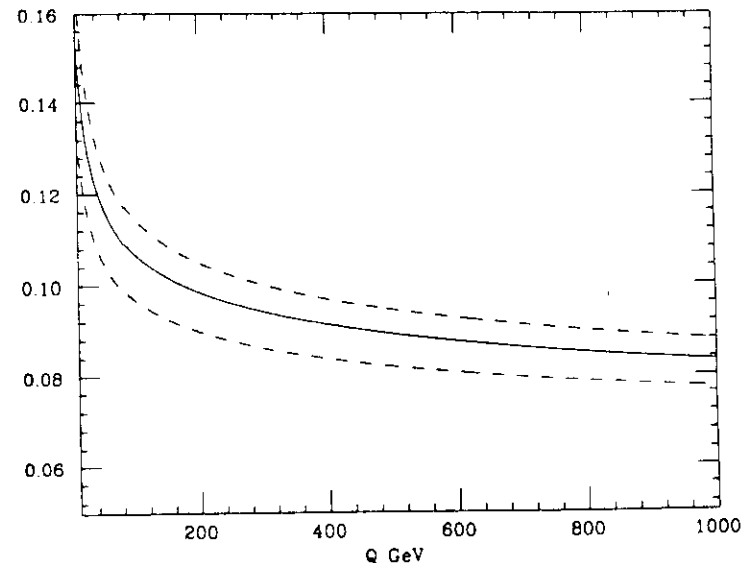

Figure 8: Figure showing $\alpha_s(Q)$ as a function of Q. The solid line indicates the central value quoted by the Particle Data Group[10], the dashed lines indicate the range of uncertainty.

that from CDHSW and CCFRR to which they apply a renormalization of order 10%, to remove the systematic disagreement with EMC. They present three fits that differ in the form of $xg(x, Q^2 = 4GeV^2)$.

$$xg(x, Q^2 = 4GeV^2) \qquad \sim (1-x)^5 \qquad (set\ 1)$$

$$\sim (1-x)^4(1+9x) \qquad (set\ 2)$$

$$\sim x^{-1/2}(1-x)^4(1+9x) \quad (set\ 3). \qquad (49)$$

They then use data from J/ψ production [28] and photon production [29] at large transverse momentum, processes that are sensitive to the shape of the gluon distribution (see below), in an attempt to distinguish between the sets. They conclude that the soft gluon distribution of *set 1* is preferred.

Set 1 has been[30] refitted using the BCDMS [13] [16] data instead of EMC [12] [15]. Here they find that the neutrino data and BCDMS are compatible and that a renormalization of the former is not needed. These authors have compared the predictions from these two sets of distributions with the data on Drell-Yan production at the ISR [31]. The BCDMS fit is preferred, but the order α_s QCD corrections to the Drell-Yan rate are quite large [7] and the α_s^2 terms are not known so any definite conclusion seems premature.

Existing deep-inelastic scattering data do not extend below $x \sim 0.01$ and cover a very small range of Q^2 at small x. This is a potential problem since for some applications it is necessary to know the parton distributions in this region. Recall that $x_1 x_2 > \hat{s}/s$ where $\hat{s}$ (s) is the center-of-mass energy squared in the parton-parton (hadron-hadron) system. It is traditional to assume that the gluon distribution obeys

$$\lim_{x \to 0} xg(x, Q_0^2) = const. \qquad (50)$$

for some scale Q_0 of order a few GeV. However this form is unstable. When evolved to higher Q^2, it develops rapidly into a steeper form (see Figure 10). As we have seen(see Equation 36) at very small x and large Q^2, it is possible to solve the Altarelli-Parisi equations analytically. This solution is singular as $x \to 0$. It is also possible to sum to all orders in α_s the most singular terms at small x and large Q^2. This gives

$$\lim_{x \to 0, M \to \infty} xg(x, Q^2) \sim x^{-\delta} \qquad (51)$$

where, $\delta = 12\alpha_s \log(2)/\pi$, which is an even more singular form [6]. It has been suggested [6] that one should use a form for $xg(x, Q_0^2)$ that is more like the asymptotic form:

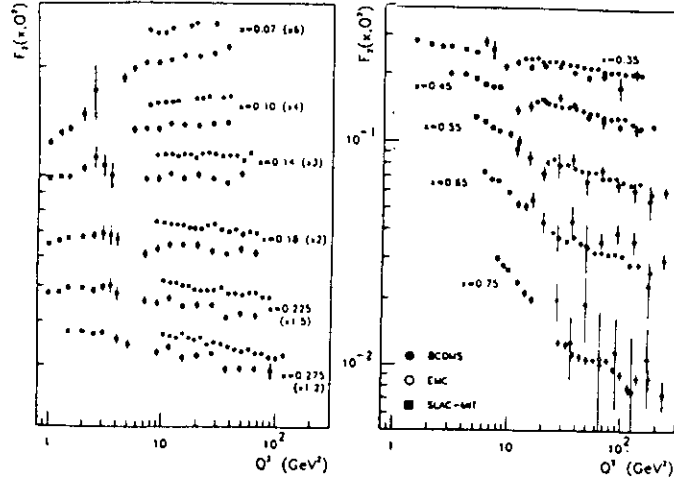$$xg(x, Q_0^2) \sim 1/\sqrt{x} \qquad (52)$$

Figure 9: A comparison of $F_2(x, Q^2)$ measured in muon scattering from a proton target from the BCDMS[13] (closed dots) and EMC[12] collaborations (open circles). Also shown are data at small Q^2 (boxes) from the electron scattering experiment[14] at SLAC.
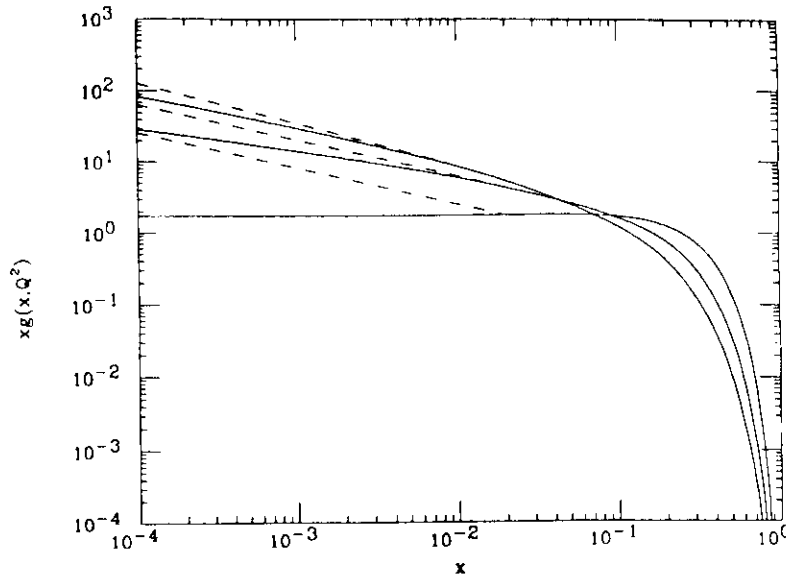
Figure 10: A comparison of the gluon distributions for fixed Q^2 as a function of x. The solid lines are EHLQ set 2 and the dashed are EHLQ2' (see text). The higher (lower) curve at small x corresponds to $Q^2 = 50(5)$ GeV^2.

is most commonly used. This argument provides the motivation for *set 3* of the MRS structure functions. It is not clear that this form is a better assumption than the traditional one, or below what value of x this form should hold. Notice that the momentum sum rule provides almost no constraint since the amount of momentum carried by gluons in the region $x < 0.01$ is small, whichever form is used there. Figure 10 compares the resulting gluon distributions at higher Q^2 that evolve from different forms at M_0^2. The two starting forms are equal for $x > 0.02$ ($Q_0^2 = 5GeV^2$) and have the forms of Equations 50 and 52 at smaller x; the first of these is the EHLQ set 2 (see above). We will refer to the other as EHLQ2' and will use it below to illustrate rates from such an extreme choice. As can be seen from Figure 10, the differences become less important at large Q^2. The uncertainties in predicted rates due to the small x problem are therefore serious only for processes sensitive to small x and small Q^2.

In order to assess the uncertainties in predicted rates quantitatively it is necessary to have set of structure functions that take into account the errors in the data that were used in making the fits. In the absence of such fits, one can attempt to estimate the uncertainties by using a range of structure functions that are compatible with existing data. Figure 11 shows the cross-section for the production of a photon at large transverse momentum. The relevant partonic processes are $g + q \rightarrow \gamma + q$ and $q + \bar{q} \rightarrow \gamma + g$. It can be seen from this plot that the uncertainties associated with the choice of structure functions are of order 25%.

Even if the structure functions and α_s were known exactly there would be some uncertainty in the QCD rates since the choice of scale Q at which they are evaluated in Equation 41 is arbitrary. If the partonic process were calculated to all orders in α_s then a change in Q would not change the result; it would merely adjust the relative sizes of the different terms in the α_s expansion. To see this note that

$$\alpha_s(Q') = \alpha_s(Q)(1 - \frac{33 - 2f}{6\pi}\log(Q/Q')\alpha_s(Q) + O(\alpha_s(Q)^2)) \qquad (53)$$

and that (see Equation 30)

$$f(x, Q'^2) = f(x, Q^2) + O(\alpha_s(Q)). \qquad (54)$$

Hence, a complete discussion of the Q^2 dependence of the calculated rates is only possible for processes where the next-to-leading order corrections to the partonic rate ($\hat{\sigma}$) is known. In the absence of such information one can vary Q^2 over a reasonable range and estimate the change in the predicted rate. The scale Q should be of order of the momentum transfer in the hard scattering process. For
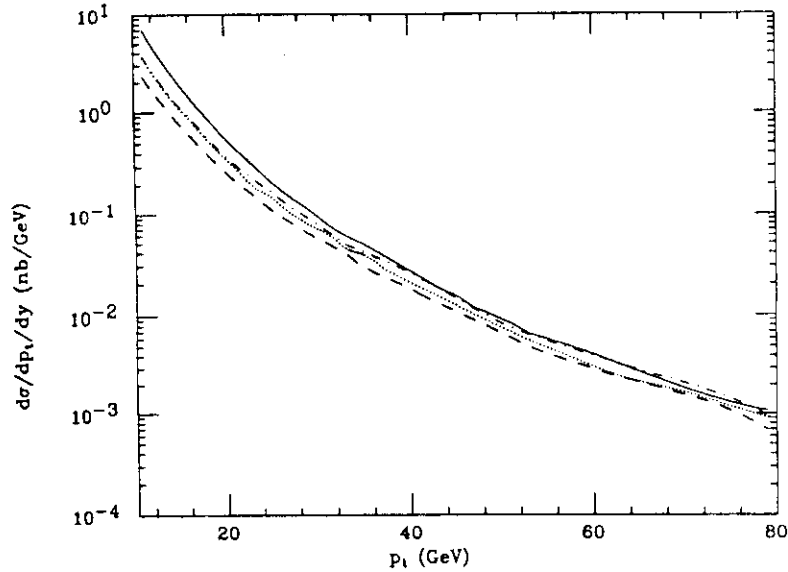
Figure 11: The cross-section $d\sigma/dp_t dy$ for the production of a photon at $y = 0$ in $p\bar{p}$ collisions at $\sqrt{s} = 1.8$ TeV for $M = \mu = p_t$. The solid, dashed, dotted, and dot-dashed lines correspond to MRS2, EHLQ2 and DFLM ($\Lambda = 260$ MeV) and EHLQ2' distribution functions respectively.

example, in the case of W production is should be of order the W mass or, in the case of photon production at large transverse momentum, it should be of order p_t.

One would expect that the Q^2 dependence of an estimated rate would be reduced if the next order corrections to $\hat{\sigma}$ are known. Keith Ellis will discuss this in the context of the production of top and bottom quarks [32]. Here I will discuss the transverse momentum distribution of W bosons. The lowest order process that contributes to the production of W bosons is $q\bar{q} \to W$. Since the incoming partons have very small (less than a few hundred MeV) transverse momentum, this process can only produce W bosons with very small transverse momentum. There are two processes at order α_s namely $q\bar{q} \to W + g$ and $gq \to W + q$ that can produce W's at large p_t; the transverse momentum of the W is balanced by that of the outgoing quark or gluon. The rate from $q\bar{q}$ is given by [33]

$$\frac{d\sigma}{dp_t dy} = 2p_t \int_{x_{min}}^{1} dx \frac{u(x, M_W^2)\bar{d}(x_1, Q^2)\sigma(\hat{s}, \hat{t}, \hat{u})}{xs + u - M_W^2} \tag{55}$$

with

$$x_1 = \frac{-xt - (1-x)M_W^2}{xs + u - M_W^2}$$

$$x_{min} = -u/(s + t - M_W^2)$$

$$\sigma(\hat{s}, \hat{t}, u) = \frac{2\pi\alpha_{em}\alpha_s(Q^2)}{9sin^2\theta_W} \frac{(t - M_W^2)^2 + (u - M_W^2)^2}{stu}.$$

Here the hatted variables apply to the partons and the unhatted to the hadrons. The W is produced with transverse momentum p_t and rapidity y. [§] The rate from the qg initial state can be obtained from this by crossing. At next order on QCD there are contributions from $q\bar{q} \to Wgg$ for example. The rate from all of the order α_s^2 processes has been computed [34] and is shown in Figure 12 as a function of Q for $p_t = 100GeV$ at $\sqrt{s} = 1.8$ TeV in $p\bar{p}$ collisions. If Q is allowed to vary over a reasonable range from $p_t/2$ to $2p_t$, it can be seen from this figure that the lowest order rate varies by a factor of order 1.8 while the order α_s^2 result changes only be a factor of 1.3. This result is typical and is to be expected if the

[§]Since the W is observed via its decay to $e\nu$ more useful experimentally is the cross-section for fixed momentum of the e. This is obtained by using the matrix element for $\bar{u}(p_u) + d(p_d) \to e(p_e) + \bar{\nu}(p_\nu) + g(p_g)$ which is given summed (averaged) over final (initial) spins and colors by

$$|M|^2 = (\frac{G_F}{\sqrt{2}})^2 \frac{2048\alpha_s M_W^6 \pi}{9(p_u - p_e - p_\nu)^2(p_d - p_e - p_\nu)^2} \frac{(p_\nu p_u)^2 + (p_e p_d)^2}{((p_e + p_\nu)^2 - M_W^2)^2 + M_E^2 \Gamma_W^2}.$$

QCD perturbation theory is reliable. (Bottom quark production at the Tevatron is an exception, here the Q dependence increases in next-to-leading order [32].)

To summarize, for a process that does not require the definition of a jet the uncertainties on the cross-section are of order 25% from structure functions (more if the process has a partonic center-of-mass energy that is less than about 40 GeV and a value of $\hat{s}/s$ less than about 10^{-4}), of order 50% from the choice of Q^2 scale if next-to-leading order QCD effects are not known and order $15n$% if the partonic process is order α_s^n. In the cases where hadronic jets are measured it is necessary to define a jet.

5 Jets and their Definition

It is well known from the analysis of e^+e^- data that the details of jet fragmentation and of the experimental jet finding algorithm can significantly effect any detailed interpretations of jet measurements, and, in particular, of attempts to use such analyses to extract the value of α_s [35].

The products from a partonic hard scattering event can include quarks and gluons as well as photons and W bosons. While the latter can be observed directly in an experiment, the former cannot. What is observed is a narrow jet of hadronic particles whose direction and total energy correlate with that of the produced quark or gluon. The simplest model of such a jet is as follows. Consider a quark with four momentum $(E, P, 0, 0)$. This will fragment into n hadrons with momenta $(E_i, p_i, p_{t_i}\cos\phi_i, p_{t_i}\sin\phi_i)$. The distribution of particles is then given by

$$\frac{dN}{dy_i dp_{t_i} d\phi_i} = f(y_i)e^{-\alpha p_{t_i}^2}, \tag{56}$$

where the rapidity distribution $f(y_i)$ is approximately constant out to its maximum value $(y_{max} \propto \log E)$ where it falls rapidly to zero. This model predicts that the jets become narrower as E increases since the average value of p_{t_i} does not increase while the average value of the momentum (p_i) parallel to the quark direction does. Furthermore the average multiplicity of particles within a jet $(<n>)$ will be proportional to $\log E$. The average value of the transverse momentum is of order 300 MeV which is similar to the scale at which $\alpha_s(Q^2)$ becomes large and QCD perturbation theory can no longer be used.

This simple model provides a reasonable description of jets at $E \lesssim$ GeV. At higher energy the width of a jet expressed in terms of its opening angle δ does not decrease as fast with energy as the naive model indicates. (The model
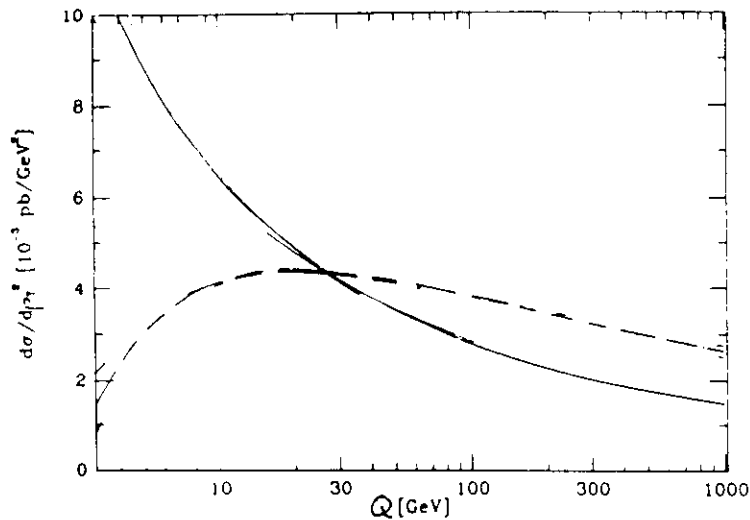

Figure 12: The dependence of the cross-section $d\sigma/dp_t^2$ for the production of a W boson with $p_t = 100$ GeV in $p\bar{p}$ interactions at $\sqrt{s} = 1.8$ TeV upon the scale Q. The solid (dashed) line is the order α_s (α_s^2) result. The DFLM ($\Lambda = 260$ MeV) structure functions are used [21] [34].

predicts $\tan\delta \sim \frac{<n><p_\perp>}{E}$). In order to understand this let us consider e^+e^- annihilation into hadrons.

At lowest order in QCD, α_s^0, the final state consists of a $q\bar{q}$ pair and one would therefore naively expect to find that the final state was dominated by 2-jet events. At next order we can get a state with an additional gluon (terms of this type contribute to the order α_s terms in Equation 20). Since the quarks and gluons hadronize into jets of particles, this would seem to imply that the ratio $\#(3\text{jets})/\#(2\text{jets})$ should be of order α_s. This is only partially true since it is necessary to define what is meant by a jet. Consider the final state of two quarks and a gluon illustrated by Figure 13. The Feynman graph contains an internal propagator which gives rise to a factor of $1/(p_2+p_3)^2$; this factor becomes singular when either the gluon becomes very soft, i.e. $p_3 \to 0$, or when it moves parallel to the outgoing quark p_2. In the calculation of the inclusive cross-section, these singularities are cancelled by the divergences also present in the radiative corrections to the final state of quark and antiquark (see Figure 14).

These soft and collinear divergences correspond precisely to those parts of phase space where a detector would only detect two jets. Consider an idealised detector consisting of a set of elements each of which covers an angular cone of opening angle δ and has an energy threshold ϵ. This detector will be incapable of resolving two jets if one of them is very soft (energy ϵ or less), or if the two jets have an angular separation which is less than δ. We can define the f to be the fraction of total cross-section in which all but a fraction ϵ of the total energy is deposited into two cones of opening angle δ. Then to order α_s,

$$(1 - f) = \frac{\sigma_{3-jet}}{\sigma_{total}} \tag{57}$$

provides a definition of the three jet fraction.

We can calculate this fraction as follows. Working in the center-of-mass of the e^+e^- system and defining $x_i = 2E_i/\sqrt{s}$, where E_i is the energy of the outgoing quark or antiquark(see Figure 13),the differential cross-section for the three parton final state can be written as

$$\frac{1}{\sigma_{total}}\frac{d\sigma}{dx_1 dx_2} = \frac{2\alpha_s}{3\pi}\frac{x_1^2 + x_2^2}{(1 - x_1)(1 - x_2)} \ . \tag{58}$$

Notice that this is singular when either x_1 or x_2 is zero which corresponds to the configuration where the gluon is soft ($x_1 \sim x_2 \sim 1$) or hard and parallel to one of the quarks (either $x_1 \sim 1$ or $x_2 \sim 1$). Hence [36]

$$(1 - f) = \int_{\epsilon,\delta} \frac{1}{\sigma_{total}}\frac{d\sigma}{dx_1 dx_2}$$
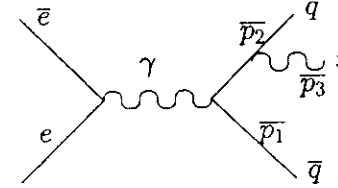

Figure 13: Feynman diagram showing a contribution to the three jet final state described by Equation 58.

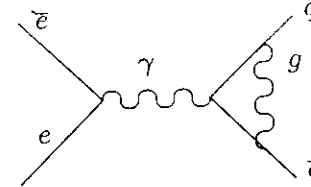Figure 14: Feynman diagram showing a virtual correction to the total cross-section in e^+e^- annihilation.
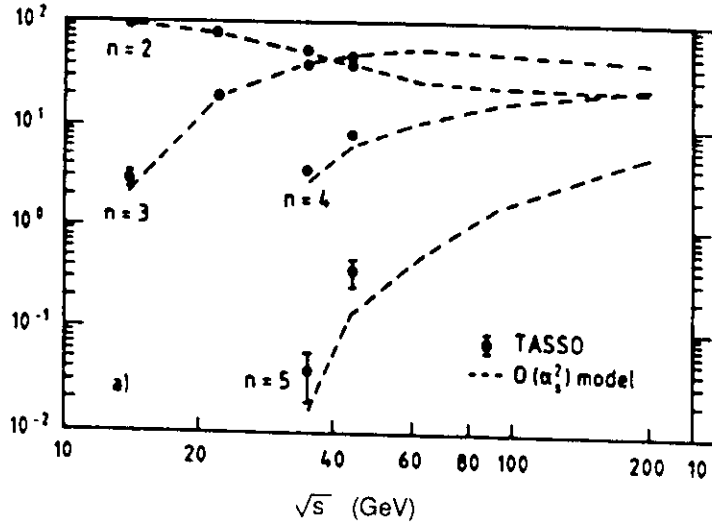
$$= \frac{4\alpha_s}{3\pi}(4 log(1/\delta) log(1/2\epsilon) - 3 log(1/\delta) + \pi^2/3 - 7/4).$$

Notice that as ϵ and δ become very small the logarithms in this expression can become very large. Ultimately the perturbation expansion in α_s breaks down since there are terms in next order which are of order $\alpha_s^2 log^2(1/\delta)$. Since this is not small compared with $\alpha_s log(1/\delta)$, the expansion is not reliable. The situation can then be improved by resumming these large logarithms to all orders.

The "fraction of three jet events" is therefore seen to depend on the jet definition. Furthermore this result shows that jets shrink only logarithmically as the energy rises (recall that α_s fall logarithmically with the energy). Another example of a jet definition in e^+e^- is as follows [37]. Suppose that n particles are produced with momenta p_i and form the invariant mass of pairs of particles:

$$M_{ij}^2 = (p_i + p_j)^2. \tag{59}$$

If $M_{ij} < M_{cut}$ then combine particles i and j into a pseudoparticle a: $p_a = p_i + p_j$. There are now $n - 1$ "particles". Iterate the procedure until no more particles can be combined. Th number of jets in the event is then equal to the number of remaining pseudoparticles. Then the n-jet cross-section varies as

$$\sigma^n \sim \alpha_s^{n-2}(M_{cut}) log^{n-2}(\sqrt{s}/M_{cut}) . \tag{60}$$

Hence if M_{cut} is held fixed the 3 jet fraction will increase with $\sqrt{s}$. This is illustrated in Figure 15.

In a hadron-hadron collision the total energy in the parton scattering is not known *a priori* and hence the parameter ϵ is irrelevant. One could define jets in terms of a fixed angular cone. Experimentally and theoretically the best definition is in terms of a cone in rapidity and azimuth. Choose some direction then define the energy of a jet in that direction to the energy inside a cone of fixed ΔR defined by

$$\Delta R = \sqrt{(\delta\phi)^2 + (\Delta\eta)^2} \tag{61}$$

where $\Delta\phi$ and $\Delta\eta$ are the distance of the energy flow from the jet direction in azimuth and rapidity. There is some minimum value of ΔR that arises from the hadronization of a single parton and from the finite resolution of detectors; a value of order 0.7 is often used [38]. I will assume that $\Delta R < \pi/2$.

At order α_s^2 there are processes such as $g + g \rightarrow g + g$ and $q + q \rightarrow q + q$ that give rise to two partons in the final state in a hadron-hadron collision. If these partons emerge at large p_t, they will give rise, after hadronization, to jets of hadrons. At this order the two partons must be separated by $\Delta\phi = \pi$, and hence

Figure 15: The relative sizes of the 2, 3,4,and 5 jet cross-section in e^+e^- annihilation as a function of $\sqrt{s}$[37] .

the final state will consist of 2 jets. The jet cross-section predicted by perturbative QCD is given simply by these $2 \to 2$ processes and does not depend on ΔR. The rate does depend rather strongly on the choice of Q^2; see Figure 16.

At order α_s^3 there are three parton final states arising from processes such as $g + g \to g + g + g$. This partonic final state could give rise to either a 2-jet or 3-jet final state depending upon the separation between the partons, *i.e.*

$$\frac{\#3 - jet}{\#2 - jet} \sim \alpha_s f(\Delta R). \tag{62}$$

The inclusive jet cross-section calculated to this order will now depend on ΔR. This is shown in Figure 17. As expected the Q^2 dependence of the cross-section is reduced when the order α_s^3 terms are included; the range of uncertainty shown on Figure 16 is reduced by about one third [39]. Notice that this calculation must include not only the three-parton final states, but also the virtual (order α_s^3) corrections to the two-parton final states. This is necessary because there are infra-red divergences in the three-parton final state that arise when one parton is very soft. These divergences cancel against those in the virtual diagrams.

Many searches for new physics in hadron-hadron collisions are limited by background from multi-jet final states. For example, one method of searching for the top quark [40] is to look for a lepton and jets arising from the production of a $t\bar{t}$ pair followed by the decays $t \to e^+\nu b$ and $\bar{t} \to \bar{b}d\bar{u}$. The background to this arises (at least for top masses larger than 60 GeV or so) for the final state $W + jets$. It is therefore vital to have good estimates of the multi-jet rates.

It is possible to use a partonic calculation to compare jet data with QCD or to estimate background rates. In this case, the theoretical prediction is taken from a partonic calculation done to some fixed order in α_s. It is important to realize that such a calculation depends not only on α_s but also on the cut-off parameters p_0 and R_0 that go into the definition of a jet. A fully correct treatment of this is, in fact, only possible in the context of a complete higher order calculation (*c.f.* previous paragraph). If one needs, for example, the four jet final state that occurs at order α_s^4, one must calculate the two loop corrections to the 2-jet final state and the one loop corrections to the 3-jet final state. In practice, the tree level results can be used (α_s^2 for 2-jet, α_s^3 for 3-jet *etc.*) together with the cutoffs. While these results can be used for estimating rates, they cannot be used for making precise QCD tests involving the comparison of final states with different numbers of jets. Recently there has been much progress in calculating these tree level rates. The exact partonic matrix elements are known for all the processes contributing to 3-parton [41] and 4-parton [42] final states. An algorithm has also been developed [43] that enables the n-parton matrix elements
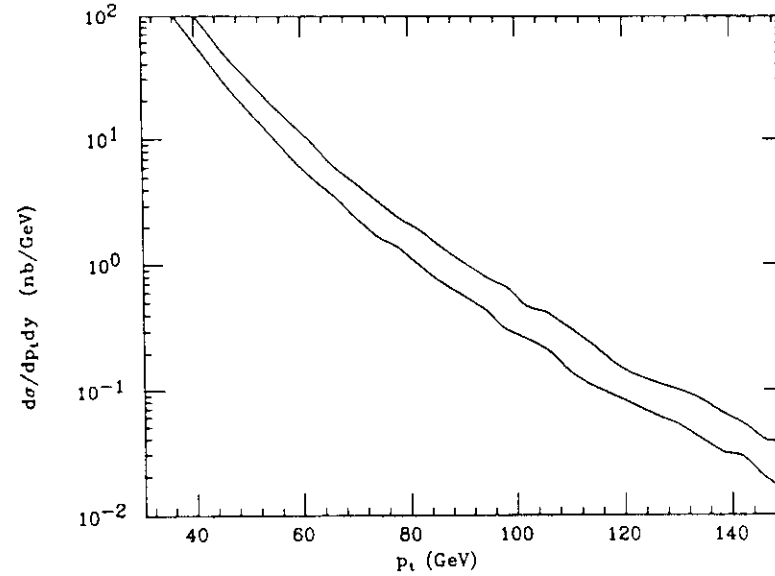

Figure 16: The cross-section $d\sigma/dp_\perp dy$ for the production of a jet at $y = 0$ in $p\bar{p}$ collisions at $\sqrt{s} = 1.8$ TeV. The curves correspond to the EHLQ2 set distribution functions with $\mu = M = p_t/2$ (upper curve) and $\mu = M = 2p_t$ (lower curve).
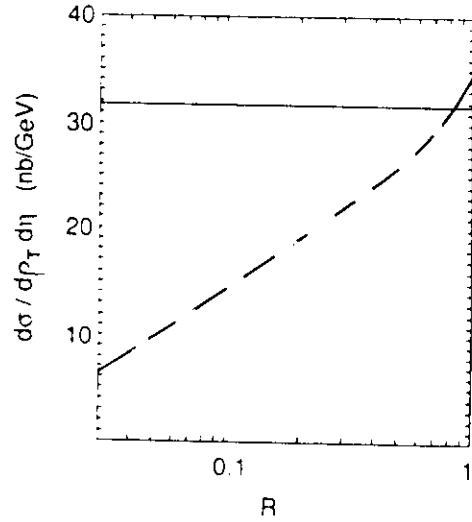
to be computed recursively. The exact matrix elements are very complicated and slow to evaluate for more than three jets. Nevertheless, approximations [44] have been developed that are accurate to 10% or better for the 4–jet and 3–jet final states and can be extended with some confidence to the final states with five or more jets. These fixed order calculations should be reliable provided that all of the jets are of approximately the same p_t. If $\alpha_s(p_t^{max})log(p_t^{max}/p_t^{min}) \sim 1$ or $\alpha_s log(2\pi y_{max}/\Delta R) \sim 1$, then the parton calculation ceases to be reliable. Here p_t^{max} (p_t^{min}) is the transverse momentum of the stiffest (softest) parton, y_{max} is the range of rapidity covered by the detector and ΔR is the separation in rapidity-phi space of the closest two partons. The latter criterion is always irrelevant given the segmentation present in current detectors.

If such a partonic calculation is to be used to compare with data, either the experimental data must be corrected back to "partonic energies", or the results of the calculation must be fed into a Monte Carlo event generator that fragments the final state quarks and gluons into the hadrons seen in the detector. The advantage of this technique is that the true QCD matrix element is used. The disadvantage is that the calculation does not include the effects of additional gluon radiation and hence of "jet broadening". There is another difficulty in that an n–jet final state is attributed to a 2 →n-parton calculation. After such a state is hadronized and passed through a jet finding algorithm, it may appear as an $(n-1)$–jet final state. Since such states are supposed to be produced by the 2 → $(n-1)$–parton scattering, there is a double counting problem.

An alternative method of calculation involves using a QCD inspired Monte Carlo generator (ISAJET [45], PYTHIA [48] or HERWIG [49] for example). Such generators usually start with the lowest order 2 → 2 calculation and then use a classical branching process to radiate more partons from these ones. This generates a multiparton final state in the so-called leading log approximation.

In order to understand how this approximation works, consider the process $g+g \to g+g+g$ which gives rise to a three parton final state. Label the momenta as follows

$$g(-p_1) + g(-p_2) \to g(p_3) + g(p_4) + g(p_5). \tag{63}$$

Then the matrix element squared for this process can be written as (summed over all spins and colors)

$$|M|^2 = N^3(N^2-1)\sum_{i>j}(p_i p_j)^4) \sum_{perms} \frac{1}{(p_1 p_2)(p_2 p_3)(p_3 p_4)(p_4 p_5)(p_5 p_1)} \tag{64}$$

where N=3. Consider the limit in which p_4 and p_5 become parallel. Then $p_4 p_5 \to$

Figure 17: Inclusive jet cross-section $d\sigma/d\eta dp_t$ for $p_t = 50 GeV$ and $\eta = 0$ in $p\bar{p}$ collisions at $\sqrt{s} = 1.8\ TeV$ as a function of the jet definition parameter ΔR. The solid (dashed) line is the order α_s^2 (α_s^3) result. The calculation was carried out in a modified version of QCD without quarks [39].

0. Then define $p_a = p_4 + p_5$ and $z = |p_4| / |p_a|$

$$|M|^2 = \frac{N^3(N^2-1)}{(p_4p_5)z(1-z)}(1+Pz^4+P(1-z)^4)\sum_{i>j}(p_ip_j)^4)\sum_{perms}\frac{1}{(p_1p_2)(p_2p_3)(p_3p_a)(p_ap_1)}$$ (65)

where the sum on i and j runs over 1,2 and 3 only, we have dropped terms that are finite as $p_4p_5 \to 0$ and P is given by

$$P = \frac{\sum_{i=1,3}(p_ap_i)^4}{\sum_{i,j=1,3;i>j}(p_ip_j)^4} .$$ (66)

Using momentum conservation one can show that $P = 1$. We can now write

$$|M|^2 = \frac{1}{(p_ap_a)}P_{gg}(z)|M_2|^2$$ (67)

where P_{gg} is the Altarelli-Parisi splitting function and M_2 is the matrix element for the process $g(-p_1) + g(-p_2) \to g(p_3) + g(p_a)$ viz

$$|M_2|^2 = N^2(N^2-1)\frac{s^4+t^4+u^4}{stu}(\frac{1}{s}+\frac{1}{t}+\frac{1}{u}) .$$ (68)

This result, which can be generalized, is the basis of the "leading log approximation".

The leading log approximation calculates $|M|^2$ for a $2 \to n$ process by selecting the pair of partons (l and m) with the lowest invariant mass and writing (as above $p_a = p_l + p_m$, and $z = |p_l| / |p_a|$

$$|M(2 \to n)|^2 \approx \frac{1}{(p_ap_a)}P_{ij}(z)|M(2 \to n-1)|^2 .$$ (69)

The procedure is then iterated so that the final expression is in terms of a number of Altarelli-Parisi factors and $M(2 \to 2)$. This approximation is good when $log(\sqrt{\hat{s}}/p_t)$ or $log(\Delta R)$ is large, where ΔR is the separation of a pair of partons.

This approximation for generating multiparton final states is used by the QCD inspired Monte Carlo generators (ISAJET [45], PYTHIA [48] or HERWIG [49] for example). Such generators usually start with the lowest order $2 \to 2$ calculation. They treat the outgoing partons as being off shell (*i.e.* they have an invariant mass of order p_t) and then allow them to "decay" with a branching probability given in terms of the Altarelli-Parisi functions. (for a review see [50]). The advantages of this approach are that it can reproduce many jet final states and that it will automatically include any jet broadening effects caused by gluon radiation. It also has no inherent problem in normalizing the rates for different

numbers of jets. The hadron (or parton) can be passed through a jet algorithm and the number of jets determined. The disadvantage of the method is that the leading log approximation does not reproduce the exact calculation for wide angle radiation (typical errors can be as large as a factor of 2 or 3 in rate) and so may not provide a good basis for comparing to multi-jet data. It is also very difficult to include higher order QCD corrections in a fully correct manner.

6   Underlying Events

In a hadron-hadron collision, events that do not contain a hard scattering make up the dominant part of the cross-section at currently available energies. These events ("minimum bias") consist of hadrons of small transverse momentum distributed uniformly in azimuth and approximately uniformly in rapidity. Since the properties of these events are not calculable in QCD, the various Monte-Carlo generators use models to simulate them. ISAJET [45] uses a Regge model [51]; PYTHIA [48] builds up the event from a large number of parton-parton scatterings each of which produces an outgoing parton of very small p_t; HERWIG [49] uses a phenomenological model based on the UA5 data [52]. All of these models contain parameters which are adjusted so that they correctly describe the data at the $Sp\bar{p}S$ collider.

When these generators are used to predict the minimum bias structure at higher energies, it is not guaranteed that they will agree, either with each other or with the data. Figure 18 shows the pseudo-rapidity distribution predicted for $p\bar{p}$ collisions at $\sqrt{s}$=1.8 TeV. It can be seen from this figure that the Monte-Carlo generators do not agree with each other and that PYTHIA provides the best agreement with the CDF data [53]. HERWIG is in reasonable agreement with the data, while ISAJET is somewhat low. However, in the PYTHIA case we have not included the contribution from the "double-diffractive" process. Including this process will lower the multiplicity slightly. It is needed at $\sqrt{s} = 630$ GeV to bring the generated values closer to those of ISAJET, HERWIG and the UA5 data. ISAJET and HERWIG do not have "double-diffractive" as a separate process. If the jet final states are also included in the HERWIG predictions, better agreement is obtained [54].

In a hadron-hadron hard scattering event, such as the production of jets or W bosons, the initial state partons in the hard scattering have evolved off shell by an amount of order the momentum transfer in the hard scattering. This evolution occurs by the emission of quarks and gluons all of which have limited transverse momentum with respect to the beam direction. These quarks and gluons then

turn into hadrons of limited p_t distributed approximately uniformly in rapidity. One therefore expects that the multiplicity of particles in the underlying event (*i.e.* that part of the event that is separated in $\phi - \eta$ space from the products of the hard scattering) should be larger in events which contain a hard scattering than in events which do not. This qualitative feature is seen in the data [55]. A comparison of this effect in the different Monte–Carlo generators is shown in Figure 19 which also shows data from CDF [53]. A comparison of this figure with Figure 18 shows that there are indeed more particles in the underlying event when a W is produced but that the distribution remains of approximately the same shape in pseudo–rapidity.
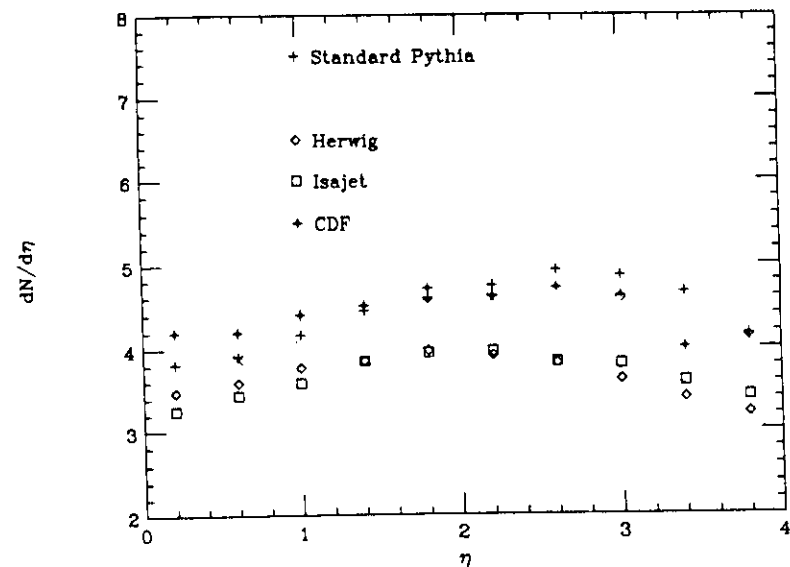
Acknowledgment

Figure 18: The distribution of multiplicity with respect to pseudo–rapidity, $dN/d\eta$, for events with no hard scattering (minimum bias) in proton–antiproton collisions at $\sqrt{s}$=1.8 TeV. The predictions of Monte–Carlo generators are compared with the CDF data [53].
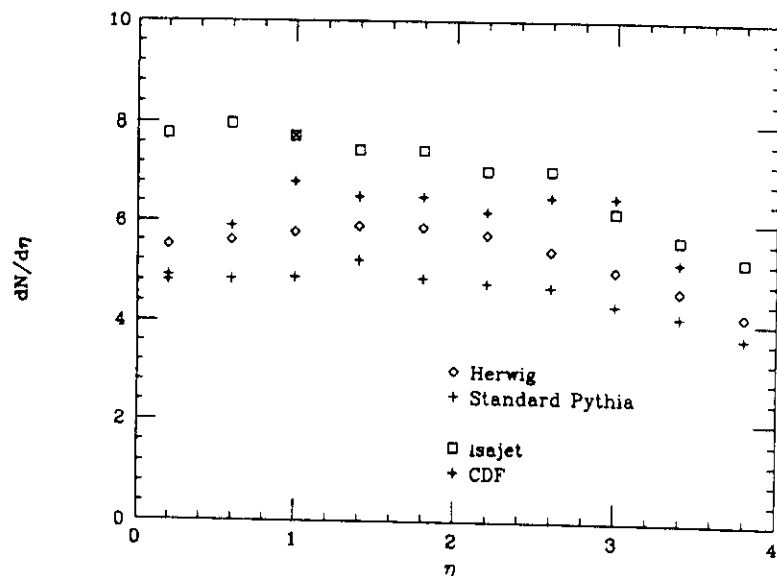
Figure 19: The pseudo-rapidity distribution $dN/d\eta$ for events in which there is a W (that decays to $e\nu$) in proton–antiproton collisions at $\sqrt{s}$=1.8 TeV. The predictions of Monte-Carlo generators are compared with the CDF data [53]. The electron from the W decay is not included.

References

[1] For a review of the QCD parton a model see G. Altarelli *Phys. Rev.* **81C**, 1 (1982),. or A. H. Mueller Lectures at the 1985 TASI (Yale University) (World Scientific Publishing Singapore, 1986). For a review of collider physics, see V. D. Barger and R.J.N. Phillips "Collider Physics" (Addison Wesley).

[2] W.A. Bardeen et al., *Phys. Rev. D* **18**, 3998 (1978).

[3] G. 't Hooft and M. Veltman, *Nucl. Phys. B* **44**, 189 (1972); C.G. Bollini, J.J. Giambiagi and A. Gonzáles Domínguez, *Nuovo Cim.* **31**, 551 (1964); J. Ashmore, *Nuovo Cim. Lett.* **4**, 289 (1972); G.N. Cicuta and E. Montaldi, *Nuovo Cim. Lett.* **4**:329 (1972).

[4] M. Dine and J. Saperstein *Phys. Rev. Lett.* **43**, 688 (1979),W Celmaster and R J. Gonsalves *Phys. Rev. Lett.* **44**, 560 (1979).

[5] G. Altarelli and G. Parisi, *Nucl. Phys.* **B126**, 298 (1977).

[6] J. Collins in "Supercollider Physics" Ed. D. Soper, World Scientific publishing (1987).

[7] G. Altarelli, et al., *Nucl. Phys.* **B143**, 521 (1978), Erratum *Nucl. Phys.* **B146**, 544 (1978).

[8] A. H. Mueller, *Phys. Rev.*, **D18**, 3705 (1978). J. Collins, D. Soper and G. Sterman, *Nucl. Phys.* **B223**, 81 (1983),*Phys. Lett.*,**109B**, 388 (1983). R. K. Ellis, et al., *Nucl. Phys.*, **B152**, 285 (1979).

[9] F. Abe et al., *Phys. Rev. Lett.* **61**, 1819 (1988).

[10] R.M. Barnett, I. Hinchliffe and J. Stirling in Review of Particle Properties *Phys. Lett.* **204B**, 1 (1988).

[11] J. Morfin and W.-K. Tung, in Proceeedings of the 1988 Snowmass Summer Study, Ed. S. Jensen. World Scientific (1989).

[12] V. Papavassiliou (EMC collaboration) Proc. of Int. Europhysics Conference on High Energy Physics, Uppsala (1987).

[13] A. Benvenuti et al., *Phys. Lett.* **195B**, 91 (1987).

[14] A. Bodek et al., *Phys. Rev.* **D20**, 1471 (1979).

[15] J.T. Aubert *et al., Nucl. Phys.* **B293**, 740 (1987); **B272**, 158 (1986), **B259**, 189 (1985); or M. Arneodo *et al., Nucl. Phys.* **B264**, 739 (1986).

[16] A. Benvenuti *et al.*, JINR-E1-87-689, 699 (1987).

[17] See, for example, F.J. Sculli, Talk at 1988 Arles Conference, June 1988, and R. Voss in Proc. of 1987 International Symposium on Lepton and Photon Interactions at High Energies, Hamburg 1987.

[18] D. Duke and J. Owens *Phys. Rev.* **D30**, 49 (1984).

[19] E. Eichten *et al., Rev. Mod. Phys.* **56**, 579 (1984).

[20] H. Abramowicz, *et al., Zeit. fur Physik* **C17**, 283 (1983).

[21] M. Diemoz, F. Ferroni, E. Longo, and G. Martinelli, CERN-TH-4757 (1987).

[22] D. Allasia *et al., Phys. Lett.* **135B**, 231 (1986); *Zeit. fur Physik* **C28**, 321 (1985).

[23] D. B. MacFarlane et al., *Zeit. fur Physik* **C26**, 1 (1984).

[24] J.V. Allaby, *et al., Phys. Lett.* **197B**, 281 (1987), CERN EP/87/225. F. Bergsma *et al., Phys. Lett.* **123B**, 269 (1983), **153B**, 111 (1985).

[25] H. Abramowicz, *et al., Zeit. fur Physik* **C35**, 443 (1987); B. Vallage, Thesis submitted to Université de Paris Sud (1984).

[26] G. Altarelli, *et al.*, CERN-TH-4978 (1988).

[27] A.D. Martin, R.G. Roberts and J. Stirling, *Phys. Rev.* **D37**, 1161 (1988).

[28] J.A. Branson *et al., Phys. Rev. Lett.* **38**, 1331 (1977); K.J. Anderson *et al., Phys. Rev. Lett.* **42**, 944 (1979); E.J. Siskind *et al., Phys. Rev.* **D21**, 628 (1980).

[29] T. Akesson, *et al., Zeit. fur Physik* **C34**, 293 (1987).

[30] A.D. Martin, R.G. Roberts and J. Stirling, *Phys. Lett.* **207B**, 205 (1988).

[31] D. Antreasyan *et al., Phys. Rev. Lett.* **48**, 302 (1982).

[32] R.K. Ellis, these proceedings.

[33] F. Halzen and W. Scott, *Phys. Rev.,* **D18**, 3378 (1978).

[34] P.B. Arnold and H. Reno *Nucl. Phys.* **B319**, 37 (1989)

[35] See, for example, S.L. Wu in *Proc. of International Symposium on Lepton-Photon Interactions*, Hamburg (1987) and references therein.

[36] G. Sterman and S. Weinberg, *Phys. Rev. Lett.,* **39**, 1436 (1977).

[37] W. Braunschwieg, *et al. Phys. Lett.* **214B**, 286 (1988).

[38] M.D. Shapiro, these proceedings.

[39] S. Ellis, D. Soper and Z. Kunszt, *Phys. Rev.* **D40**, 2188 (1989).

[40] R. Hollebeek, these proceedings.

[41] F. A. Berends, *et al., Phys. Lett.* **103B**, 124 (1982).

[42] S.J. Parke and T.R. Taylor, *Nucl. Phys.* **B269**, 410 (1986); Z. Kunszt, *Nucl. Phys.* **B271**, 333 (1986); J.F. Gunion and J. Kalinowski, *Phys. Rev.* **D34**, 2119 (1986).

[43] F.A. Berends and W.T. Giele, *Nucl. Phys.* **B306**, 759 (1988).

[44] C.J. Maxwell, *Phys. Lett.* **192B**, 190 (1987), Durham preprint DTP-88/32 (1988); Z. Kunszt and W.J. Stirling, *Phys. Rev.* **D37**, 2439 (1988); S.J. Parke and M. Mangano FNAL-Pub-88/92-T (1988).

[45] F. Paige and S. Protopopescu, in Proc. of 1986 Snowmass Summer Study on the Physics of the SSC, Ed. R. Donaldson FNAL (1987).

[46] EUROJET, B. van Eijk, in Proc. of the 5th International Workshop on $p\bar{p}$ Interactions, St. Vincent, Italy (1985).

[47] PAPAGENO, I. Hinchliffe, in preparation.

[48] H-U. Bengtsson and T. Sjostrand, *Comp. Phys. Comm.* **46** 43, (1987).

[49] G. Marchesini and B.R. Webber, CAVENDISH preprint 88/7 (1988).

[50] B. R. Webber *Ann. Rev. Nucl. and Part. Sci.* **36**, 253 (1986).

[51] V.A. Abramovskii, O.V. Kanchelli and V.N. Gribov in *Proc.* 16th International Conference on High Energy Physics, FNAL (1983), Vol. 1, p.363.

[52] C.G. Alner, *et al., Phys. Rep.* **154**, 247 (1987).